

CSI-EPT: A novel Contrast Source Inversion approach to EPT and patient-specific SAR based on B₁⁺ maps

E. Balidemaj¹, R.F. Remis², A.L van Lier³, J. Crezee¹, A.J. Nederveen⁴, A. Sbrizzi³, L.J.A. Stalpers¹, and C.A.T. van den Berg³

¹Radiotherapy, Academic Medical Center, Amsterdam, Netherlands, ²Faculty of Electrical Engineering, TU Delft, Delft, Netherlands, ³Radiotherapy, UMC Utrecht, Utrecht, Netherlands, ⁴Radiology, Academic Medical Center, Amsterdam, Netherlands

Introduction & Theory: Electric Properties Tomography (EPT) [1] and the more recent Local Maxwell Tomography [2] are MR-based techniques to reconstruct dielectric tissue profiles (conductivity σ and permittivity ϵ_r) from measured B₁⁺ data. Knowledge about these profiles can be exploited in a variety of ways and is essential to accurately describe the various electromagnetic field effects that can take place during an MRI scan. The profiles are required to determine the SAR deposition during MRI measurements [1], for example, and accurate dielectric maps might further serve for patient-specific Hyperthermia Treatment Planning. Standard EPT is based on Maxwell's equations in differential or integral form and assumes piecewise constant media [1,3]. This assumption may result in significant reconstruction errors especially near interfaces between different tissue types. A typical example is shown in Figure 1, where the reconstructed σ profile of a female adult model (Ella model, IT'IS Foundation) is reconstructed based on EPT. In this work, our aim is to improve the dielectric reconstruction results by treating EPT as a full electromagnetic inversion problem. In particular, we apply the so-called Contrast Source Inversion (CSI) method [4] to B₁⁺ data to obtain the desired dielectric tissue profiles. CSI has been applied to a wide range of inverse scattering problems [4], where one usually measures the field outside a reconstruction domain of interest. In MRI, however, we have the unique advantage that we are able to measure B₁⁺ fields inside the object itself. Thus, we expect that CSI can be used to reconstruct the dielectric maps with high accuracy. Moreover, CSI-EPT reconstructs the unknown electric field as well and is therefore a promising method to determine the patient-specific SAR deposition.

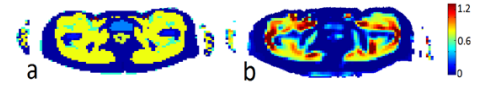


Figure 1: Actual σ -map (a) and reconstructed σ -map (b) based on standard EPT.

In particular, we apply the so-called Contrast Source Inversion (CSI) method [4] to B₁⁺ data to obtain the desired dielectric tissue profiles. CSI has been applied to a wide range of inverse scattering problems [4], where one usually measures the field outside a reconstruction domain of interest. In MRI, however, we have the unique advantage that we are able to measure B₁⁺ fields inside the object itself. Thus, we expect that CSI can be used to reconstruct the dielectric maps with high accuracy. Moreover, CSI-EPT reconstructs the unknown electric field as well and is therefore a promising method to determine the patient-specific SAR deposition.

Materials & Methods: As opposed to standard EPT, CSI-EPT is based on two domain integral representations for the electromagnetic field. In particular, the first integral representation (1), known as the *data equation*, relates the measured field \mathbf{f} to the contrast source \mathbf{w} via the electric-current to magnetic field Green's tensor \mathbf{G}^{HJ} of the background medium. The contrast source $\mathbf{w}(\mathbf{x}) = \chi(\mathbf{x})\mathbf{E}(\mathbf{x})$ consists of the product of the unknown dielectric profile function $\chi(\mathbf{x}) = \epsilon_r(\mathbf{x}) - 1 - j\sigma(\mathbf{x})/(\omega\epsilon_0)$ and the unknown total electric field \mathbf{E} . Although we do not know the electric field, we do know that this field must satisfy Maxwell's equations. In integral form, this amounts to requiring that the electric field strength satisfies the so-called *object equation* (2). This second equation

$$\mathbf{f}(\mathbf{x}) = \int_{x' \in D} \underline{\underline{\mathbf{G}}}^{\text{HJ}}(\mathbf{x}, \mathbf{x}') \mathbf{w}(\mathbf{x}') dV \quad (1)$$

therefore acts as a kind of constraint for the data equation. In Eq. (2), \mathbf{G}^{EJ} is the electric-current to electric field Green's tensor and \mathbf{E}^{inc} is the electric field inside an empty coil. In CSI-EPT, we now minimize an objective function which measures the discrepancy in the data and object equation. The contrast source and contrast function are updated in an iterative fashion by minimizing the objective function at every iteration. After a successful completion of the algorithm, the contrast function and contrast source have been reconstructed. Since the contrast source consists of the product of the electric field strength and the contrast function, the electric field is therefore reconstructed as well. Mathematical details about the updating procedure in CSI can be found in [4].

In Eq. (2), \mathbf{G}^{EJ} is the electric-current to electric field Green's tensor and \mathbf{E}^{inc} is the electric field inside an empty coil. In CSI-EPT, we now minimize an objective function which measures the discrepancy in the data and object equation. The contrast source and contrast function are updated in an iterative fashion by minimizing the objective function at every iteration. After a successful completion of the algorithm, the contrast function and contrast source have been reconstructed. Since the contrast source consists of the product of the electric field strength and the contrast function, the electric field is therefore reconstructed as well. Mathematical details about the updating procedure in CSI can be found in [4].

Results & Discussion: As a proof of principle, we illustrate the performance of CSI-EPT for a 2D problem in which we attempt to reconstruct the dielectric profiles in a slice through the abdomen region of the Ella model. The actual σ and ϵ_r profiles are shown in Figs. 2a and 2f, respectively. A forward modelling code computes the corresponding B₁⁺ field as generated by 4 line sources (driven at 128MHz) located symmetrically around the object to mimic a quadrature driven coil. This field now serves as an input for CSI-EPT. Note that here we assumed that perfect B₁⁺ transmit phase is available without receive phase contamination, although this might be addressed by incorporation of the transceive phase, $\arg(B_1^+ B_1^-)$, in the algorithm. After 100 iterations, we obtain the reconstructed σ and ϵ_r maps shown in Figs. 2b and 2g. These maps show a resemblance with the actual maps, but are too smooth and small structures are not yet visible. However, if we increase the number of iterations to 10000 (computation time: 9 minutes), we observe a dramatic improvement and the discrepancy

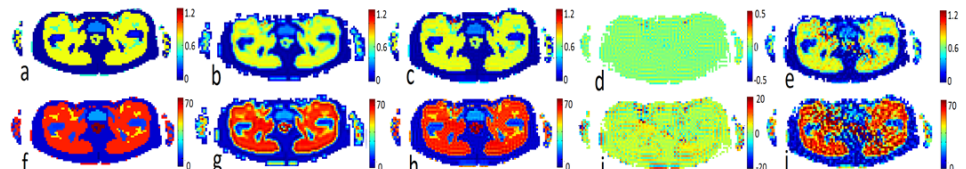


Figure 2: Original σ and ϵ_r profiles (a and f), reconstructed profiles obtained after 100 iterations (b and g) and 10000 iterations (c and h), the difference between the reconstructed and original profiles after 10000 iterations (d and i), reconstructed profiles after 1000 iterations with noisy (SNR 20) B₁⁺ data (e,j).

between the reconstructed (Figs. 2c and 2h) and actual maps is very small (see Figs. 2d and i). From Figs. 2a,f,c, and h we also observe that the reconstruction near tissue interfaces is very reliable. To study the sensitivity of CSI-EPT, we added Gaussian noise to the B₁⁺ data and present the reconstructed profiles in Figs. 2e and 2j. As expected, lower-quality reconstruction results are obtained (Figs. 2e and 2j), but the profiles are still recognizable. We note that the effects of noise can be further suppressed by including total variation regularization in CSI-EPT [4]. Finally, in Figure 3 we show the amplitude and phase of the electric field based on the actual model (Figs. 3a and 3b) and reconstructed model of Fig. 2e,j (see Figs. 3c and 3d). These results confirm that CSI-EPT may serve as a reliable tool to determine the patient-specific SAR deposition.

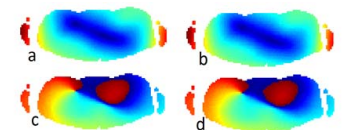


Figure 3. Normalized E-field magnitude (a,b) and phase (c,d) based on the actual profile of Figs.2a,f, left column, and the reconstructed profile of Figs.2e,j, right column.

Conclusions: We have presented a new CSI-EPT approach to retrieve the dielectric maps from B₁⁺ data. In our method, we treat the EPT problem as a full electromagnetic inversion problem and utilize the Contrast Source Inversion method to obtain the dielectric tissue parameters. The presented results demonstrate the ability of CSI-EPT to reconstruct heterogeneous dielectric profiles that are reliable at tissue boundaries and small structures. Furthermore, the electric field strength is also reconstructed in CSI. This implies that the SAR deposition can be determined as well. The method can be extended to 3D problems as shown in several CSI studies.

References [1] Katscher *et al.*, IEEE 28:1365-75, 2009. [2] Sodickson, ISMRM 2012, 387 [3] Van Lier, MRM 2011. [4] Van den Berg, P. M., PIER 34, 189–218, 2001.